

This discussion paper is/has been under review for the journal Atmospheric Measurement Techniques (AMT). Please refer to the corresponding final paper in AMT if available.

CO₂-gradient measurements using a parallel multi-analyzer setup

L. Siebicke¹, G. Steinfeld², and T. Foken¹

¹Department of Micrometeorology, University of Bayreuth, Bayreuth, Germany

²Institute of Physics, ForWind, Center for Wind Energy Research, Carl von Ossietzky University of Oldenburg, Oldenburg, Germany

Received: 17 August 2010 – Accepted: 24 September 2010 – Published: 11 October 2010

Correspondence to: L. Siebicke (lukas.siebicke@uni-bayreuth.de)

Published by Copernicus Publications on behalf of the European Geosciences Union.

4383

Abstract

Accurate CO₂ concentration gradient measurements are needed for the computation of advective flux terms, which are part of the full Net Ecosystem Exchange (NEE) budget equation. A typical draw back of current gradient measurement designs in advection
5 research is the inadequate sampling of complex flow phenomena using too few observation points in space and time. To overcome this draw back, a new measurement design is presented which allows the parallel measurement of several sampling points at a high frequency. Due to the multi-analyzer nature of the design, inter-instrument
10 bias becomes more of a concern compared to conventional setups. Therefore a statistical approach is presented which allows for accurate observations of concentration gradients, which are typically small in relation to analyzer accuracy, to be obtained. This bias correction approach applies a conditional, time dependent signal correction. The correction depends on a mixing index based on cross correlation analysis, which characterizes the degree of mixing of the atmosphere between individual sam-
15 ple points. The approach assumes statistical properties of probability density functions (pdf) of concentration differences between a sample point and the field average which are common to the pdf's from several sample points. The validity of the assumptions made was successfully verified by Large Eddy Simulation (LES) using the model PALM. The study presents concentration time series before and after correction, measured at
20 a 2 m height in the sub-canopy at the FLUXNET spruce forest site Waldstein-Weidenbrunnen (DE-Bay), analyzes the dependence of statistical parameters of pdf's from atmospheric parameters such as stratification, quantifies the errors and evaluates the performance of the bias correction approach. The improvements that are achieved by applying the bias correction approach are one order of magnitude larger than possible
25 errors associated with it, which is a strong incentive to use the correction approach. In conclusion, the presented bias correction approach is well suited for – but not limited to – horizontal gradient measurements in a multi-analyzer setup, which would not have been reliable without this approach. Finally, possible future improvements of the bias correction approach are outlined and further fields of application indicated.

4384

1 Introduction

Advection is a part of Net Ecosystem Exchange (NEE) of carbon dioxide, the determination of the latter being a primary focus of a world wide network of vegetation-atmosphere exchange measuring stations, the FLUXNET (Baldocchi et al., 2001). Not only are reliable measurements of advection lacking for most FLUXNET sites, but they continue to be a challenge even for specialized advection research experiments (e.g. Aubinet et al., 2003; Staebler and Fitzjarrald, 2004; Feigenwinter et al., 2008; Aubinet et al., 2010). Advection remains further to be a major reason for the night flux problem (Finnigan, 2008). Mathematically, scalar advection is the product of the mean spatial gradient of a scalar – CO₂ in the case of the current study – and the mean wind velocity, i.e. scalar transport with the mean flow. Advection is typically addressed as vertical advection (Lee, 1998; Baldocchi et al., 2000) and horizontal advection (Baldocchi et al., 2000; Aubinet et al., 2003).

There are two main conceptually different reasons why valid and representative advection measurements are difficult to obtain. One is the instrument related accuracy, with which scalar gradients and wind vectors of the mean flow can be measured. The other reason being undersampling of complex flow phenomena due to limited resources of real world experiments, thus yielding measurements which are not representative for a spatial (volume) and temporal (time period) mean but for a point only.

Vertical and horizontal advection pose different measurement challenges. With regards to vertical advection, reliable vertical CO₂ concentration gradients can be obtained due to vertical concentration gradients which are relatively large compared to sampling uncertainties. Measurements of vertical wind velocity are difficult to obtain, both for reasons of accuracy, precision, and resolution of sonic anemometers and particularly for reasons of the limited spatial representativity of a point measurement. Spatially representative measurements of vertical wind speed can never be obtained from a single point measurement in complex flow, due to theoretical reasons; therefore multi-tower measurements – possibly in combination with airborne measurements

4385

– are being suggested to improve spatial representativity of vertical wind measurements (e.g. Mahr, 2010). Alternatively, the vertical wind velocity measurement problem is avoided by using a mass continuity approach, i.e. inferring vertical motion from horizontal divergence (e.g. Vickers and Mahr, 2006; Montagnani et al., 2010) or a combination of the mass continuity approach and modeling (Canepa et al., 2010). Regarding horizontal advection, measurements of horizontal wind speed can be obtained with sufficiently high accuracy with sonic anemometers, even though they are often not spatially representative. Contrary, horizontal gradients are very difficult to measure with the required accuracy, because mean gradients are small in relation to instrument related uncertainty and difficult to measure at a large enough number of locations with a sufficiently high temporal resolution.

It is the main aim of this study to provide improvements for the measurement of horizontal CO₂ concentration gradients by means of a better temporal and potentially better spatial resolution. An improved resolution is needed for advection measurements in heterogeneous forests as could be shown by analyzing the effects of spatial heterogeneity and short lived phenomena on mean horizontal CO₂ concentration gradients (Siebicke et al., 2011).

The most commonly used setup for horizontal gradient measurements is based on a switching valve system (e.g. Burns et al., 2009), which uses a single closed-path infrared gas analyzer to sample several points one after the other (“sequential approach”), returning to the same sample point once every few minutes. There is an inherent tradeoff between achievable spatial and temporal resolution. The main benefit of this setup is a common analyzer for a number of sample locations, reducing the risk of bias between those points. The current study utilizes a multi-analyzer setup, featuring an individual closed-path infrared gas analyzer for every measurement point, enabling simultaneous measurements of all points (“parallel approach”) with a high frequency. Temporal resolution is no longer parasitic to spatial resolution, the latter depending on available resources only. With ten individual analyzers used, the spatial resolution is on the order of a sequential system. Thus the system described is capable

4386

avoid any possible bias of the concentration measurement from differences in pressure or temperature (sample air temperature, ambient analyzer temperature, radiation). All CO₂ closed-path gas analyzers shared a common housing in a central position with controlled conditions resulting in a constant common temperature and common pressure regime. Moreover, all analyzers shared a common tailor-made automatic calibration system, using high precision reference gases (accuracy 0.1 μmol mol⁻¹). The calibration routine included an automatic calibration every 4 h using two reference concentrations. In addition to factory calibration, each instrument's polynomial calibration function was established on site, using multiple standards. The polynomial was checked before and during the experiment.

Individual technical measures taken to avoid systematic inter-instrument bias include the following:

- The length of tubing connecting each sample point with the corresponding gas analyzer was exactly 75 m for every point. Sample tubes used were of polyethylene-aluminum composite structure, model DEKABON 1300-M060X (Serto AG, Fulda-brück, Germany) with an inner diameter of 4 mm.
- Large diameter line intake air filters were checked regularly and replaced synchronously at all points, if necessary.
- Common ambient temperature and pressure for all gas analyzers and calibration unit, including radiation protection, active automatic temperature control by heating and cooling as well as carefully designed ambient air circulation.
- Quality control of performance of automatic temperature control system, making sure that ambient air temperatures measured at several points surrounding the gas analyzers remain within acceptable range.
- Temperature adaptation for sample lines, to allow the temperature of sample air in all sample lines to equilibrate to a common temperature prior to entering the analyzer.

4389

- Common temperature and radiation shielding for reference gases.
- Minimization of dead volumes in calibration and valve system to ensure turbulent flow conditions and avoid contamination by previous samples.
- Flow rate of 2 L min⁻¹ (Reynolds number $Re = 2520$) above critical flow rate of 1.8 L min⁻¹ at critical Reynolds number ($Re_{crit} = 2320$) to ensure turbulent flow conditions in all tubes, at the same time keeping the flow rate as low as possible to minimize pressure drop across the system.
- Regular flow rate check and adjustment for all sample lines.
- Bypass system to avoid back pressure effects during calibration, featuring a low pressure drop bypass flow rate control device to ensure minimum necessary bypass flow and avoid possible reverse flow and sample contamination by ambient air.
- One common pump downstream of the analyzers to reduce effects of the pump on the concentration signals and to guarantee common pressure for all analyzers, assuming equal pipe geometry of all sample lines.
- Automatic control of constant overall system flow rate by mass flow controller.
- Passive system to allow for pressure equilibration between sample cells of individual gas analyzers by connecting all analyzer outlets to a manifold with a sufficiently large diameter.
- Pre-assembly measurement and evaluation of the pressure drop caused by individual system components to ensure that associated errors of the CO₂ concentration measurements are below accepted threshold.
- Vacuum and over pressure assisted leak check for the complete system to rule out sample contamination by ambient air.

4390

2.3 Data set

The data set was collected during the second intensive observation period (IOP2), 1 June to 15 July 2008 of the EGER (“ExchanGE processes in mountainous Regions”) experiment (Foken et al., 2011). 24.6 days worth of data were used for the analysis, i.e. 1181 half hourly values taken from a window of 32.0 days (11 June to 13 July). Periods were excluded from the analysis when instruments were powered off or obviously malfunctioning.

2.4 Theoretical considerations regarding concentration differences

2.4.1 Bias

An observed concentration difference between two spatially separated sample points is the sum of a concentration difference originating from a natural atmospheric concentration gradient and the inter instrument bias, the latter being determined by systematic (bias) and random error of the individual instruments. We will refer to this composite concentration difference also as a concentration offset, Δc . While random error of the instruments is a minor concern in the current study due to sufficiently long averaging period, instrument bias can be reduced by calibration against known standards. The calibration procedure used in this study was outlined in Sect. 2.2. The remaining bias is the sum of the error of the calibration plus the instrument drift between two consecutive calibration events. This remaining bias cannot be removed by calibration since it is intrinsic to the calibration procedure itself. However, a statistical approach detailed in Sect. 2.7 can help to distinguish between remaining bias and concentration differences originating from natural gradients based on the observed signal.

2.4.2 Natural concentration differences

To separate concentration differences originating from natural gradients between two spatially disjunct (i.e. up to a few tens of meters) sample points from instrument bias

4391

the following assumption is made and is the basis for bias correction used in the current study: for certain meteorological conditions the concentration time series observed simultaneously at the two locations can be statistically linked to a reference concentration which is common to both sample locations. To be more precise, under the condition of well mixed, i.e. sufficiently turbulent atmospheric conditions (hereafter “mixed” conditions) the concentration difference between the two locations which is most likely to be observed is zero. If this statement is true for the concentration difference between any two points, it can also be applied to the difference between the concentration at one sample location c_i , and the spatial average concentration of the sample point field $\bar{c}(t)$ at a given time t . $\bar{c}(t)$, which serves as a reference concentration, describes the background concentration of the sample point field at time t using the median field concentration according to Eq. (1)

$$\bar{c} = \begin{cases} c_{\frac{n+1}{2}} & n \text{ odd} \\ \frac{1}{2} (c_{\frac{n}{2}} + c_{\frac{n}{2}+1}) & n \text{ even} \end{cases} \quad (1)$$

with n observations $(c_1(t), c_2(t), \dots, c_n(t))$.

The statistical measure describing the concentration difference most likely to be observed is the mode of the probability density distribution (pdf) of the concentration differences $c_i(t) - \bar{c}(t)$, which is assumed to be close to zero under the condition of well mixed i.e. sufficiently turbulent atmospheric conditions.

This is illustrated in Fig. 2b for two hypothetical time series $c_1(t) = 7, 6, 5, 5, 8, 5, 4, 6, 5, 6$ and $c_2(t) = 7, 6, 7, 5, 3, 5, 4, 5, 6, 5$, displayed in Fig. 2a. The characteristics of turbulence justify the assumed mode of the pdf to be close to zero, i.e. turbulence consists of temporal perturbations of a mean state which are stochastic and relatively short in duration compared to the observation period. The mode is zero even though the time series $c_1(t)$ and $c_2(t)$ given in Fig. 2a have a different mean (temporal mean indicated by overline): $\overline{c_1(t)} = 5.7$ and $\overline{c_2(t)} = 5.3$, and even though the mean of the concentration difference $c_i(t) - \bar{c}(t)$ is different from zero: $\overline{c_1(t) - \bar{c}(t)} = 0.2$ and

4392

the sink at a 27.5 m height had a strength of $-8.8 \times 10^{-8} \text{ kg m}^{-3} \text{ s}^{-1}$ (approx. equivalent to maximum daytime Net Ecosystem Exchange of $-20 \mu\text{mol m}^{-2} \text{ s}^{-1}$ observed at the site).

For case B no additional concentration gradient was prescribed but a horizontal gradient in the source strength s along the y -direction was introduced (Fig. 3b, see right axis). With a basic source strength of $4.4 \times 10^{-8} \text{ kg m}^{-3} \text{ s}^{-1}$ at $y = 0$ and $y = L_y$, the source strength gradient $\frac{\partial s}{\partial y}$ was $5.5 \times 10^{-11} \text{ kg m}^{-4} \text{ s}^{-1}$ for $y \leq \frac{L_y}{2}$, while it was $-5.5 \times 10^{-11} \text{ kg m}^{-4} \text{ s}^{-1}$ for $y > \frac{L_y}{2}$. Case B has a mean source strength of $8.8 \times 10^{-8} \text{ kg m}^{-3} \text{ s}^{-1}$, which is equivalent to the constant source strength in case A (again approx. equivalent to maximum daytime Net Ecosystem Exchange of $-20 \mu\text{mol m}^{-2} \text{ s}^{-1}$ observed at the site), with 50% of that value at the domain borders $y = 0$ and $y = L_y$ and 150% of that value in the center of the domain at $\frac{L_y}{2}$. Source and sink height and sink strength of case B are equivalent to case A.

The release and the extraction of the scalar quantity started after a spin-up time of 2 h. The simulations were initialized with wind profiles obtained from a one-dimensional prerun. The geostrophic wind (u_g, v_g) was prescribed as ($3 \text{ m s}^{-1}, 0 \text{ m s}^{-1}$) while u and v correspond to the x - and y -direction, respectively. The roughness length was 0.1 m. Initially, the potential temperature was constant up to a height of 400 m. At larger heights the potential temperature increased by 0.01 K m^{-1} . At the bottom boundary of the model domain a near-surface heat flux of 0.01 K m s^{-1} was prescribed, so that a convective boundary layer developed with time. The Coriolis force was taken into account in the simulation and the Coriolis parameters used were that obtained for a geographical latitude of 55° . Time series of scalar concentration were recorded at 16 observation points within the xy -cross section of the model domain ($3.2 \times 3.2 \times 2 \text{ km}$, $640 \times 640 \times 256$ grid points, grid stretching in the vertical direction above 1000 m with a maximum grid size of 20 m) at a height of 17.5 m beginning from the first release of scalar quantity until the end of the LES 7200 s later. Figure 3 shows the location of the virtual observation points. The coordinates of the 16 observation points were

4395

composed out of the x -coordinates (760 m, 785 m, 810 m, 835 m) and y -coordinates (760 m, 785 m, 810 m, 835 m). Thus, the distance between two adjacent observation points along the x - or y -direction was 25 m.

2.6 Mixing index

A “mixing index” MI was formulated to quantify the degree of mixing between the real world sample points given in Fig. 1. A threshold value MI_c was then used to separate conditions which satisfy the assumption from those violating it. The mixing index MI is based on the cross correlation $R_{c_1 c_2}(\tau)$ of the simultaneous concentration time series $c_1(t)$ and $c_2(t)$ of spatially separated sample locations normalized by their mean variance σ^2 . The cross correlation function is given as

$$R_{c_1 c_2}(\tau) = \frac{1}{T_F} \int_{-T_F/2}^{T_F/2} c_1(t) \cdot c_2(t + \tau) dt \quad (2)$$

with time lag τ between concentration time series $c_1(t)$ and $c_2(t)$, T_F being the length of the time window of $c_1(t)$ and $c_2(t)$ and $\tau \in [-T_F, T_F]$. MI then writes:

$$MI = \max(|R_{c_1 c_2}(\tau)|) \cdot \left(\frac{\sigma_{c_1}^2 + \sigma_{c_2}^2}{2} \right)^{-1} \quad (3)$$

More specifically, MI was calculated using the mean cross correlation of CO_2 concentration time series c_5 and c_6 recorded at a sample point pair oriented along the terrain slope (locations M5, M6) and c_5 and c_8 recorded at a sample point pair oriented across the slope (M5, M8) divided by the mean field variance of all concentration time series c_5, c_6, \dots, c_{14} at sample locations M5, M6, \dots , M14 using a window length of $T_F = 60 \text{ min}$.

The critical mixing index MI_c was empirically inferred from the density distribution of MI given in Fig. 4a. Sensible values were found to be in the range $MI_c \in [0.06, 0.12]$,

4396

29 June 2008 without bias correction but including calibration using known reference gas standards. Figure 6b presents the same data after applying the bias correction. The comparison of the two figures clearly demonstrates that the bias correction is able to remove systematic concentration offsets between different analyzers in the uncorrected measurements (Fig. 6a). The offsets are most obvious during well mixed daytime conditions – when natural concentration differences are relatively small – and could be eliminated successfully in the bias corrected time series at all times of the day (Fig. 6b).

Inter-instrument bias leads to relatively constant offsets between individual concentration measurements $c_i(t)$ during daytime conditions (Fig. 6a), exactly matching the period of a high mixing index (Fig. 4b). The minor importance of concentration differences due to natural gradients during well mixed conditions is the reason why inter-instrument bias becomes the prominent component of observed inter-instrument concentration differences (compare also Fig. 9 and Fig. 10). Well mixed conditions with $MI \geq MI_c$ and $MI_c = 0.13$ were observed every day during the experiment, accounting for 30% of the entire data set. There are a few cases where mixed conditions are present for short isolated periods (e.g. one or two 60-minute MI values) at transition times in the early morning or sometimes in the early evening.

While Fig. 6a and 6b presented CO_2 concentration time series before and after bias correction on 29 June 2008, Fig. 7 displays an example of corresponding density distributions of concentration differences during a well mixed 60-minute period at midday of the same day, which were used during bias correction. Probability density distributions with analyzer specific non-zero distribution modes in the uncorrected data of Fig. 7a have been shifted by their mode so that the new mode of the distributions is equal to zero after bias correction (Fig. 7b). Figure 7b also emphasizes sample location specific differences of the distribution shape, such as different skewness and kurtosis, which is an effect of natural concentration gradients being unique for every sample location.

Having discussed probability density distributions above for an ideal case with mixed conditions, Fig. 8 demonstrates the effect of atmospheric stratification (ζ) and the

4401

degree of mixing (MI) on the shape of selected 60-minute probability density distributions of concentration differences, which mark typical conditions during the course of a fair weather day, 29 June 2008. Distributions of the well mixed case in Fig. 8c are unimodal and show high kurtosis. This is beneficial for the reliable estimation of the mode, which is necessary for bias correction. High kurtosis is a consequence of small natural horizontal and vertical gradients during well mixed conditions in the middle of the day. Figures 8b and 8d represent transition periods between night and day and between day and night, respectively, while Fig. 8a and 8e are examples of night time conditions, with Fig. 8e being a representative example for conditions with katabatic sub-canopy drainage flow under very stable conditions. The kurtosis of the distributions correlates with ζ (indicator for atmospheric stratification) as well as with MI (indicator for turbulent mixing), the result being that kurtosis decreases and skewness often increases with increasing stability parameter ζ and decreasing mixing index MI . This is due to large horizontal and vertical scalar concentration gradients during such conditions, also potentially causing multimodal distributions (Fig. 8b and 8d), which can lead to disambiguities concerning the relevant mode if they were to be used for bias correction, which they are not due to the mixing index condition. However, the effect of atmospheric stability ζ is not uniform, meaning that multiple modes and skewed distributions (Fig. 8b) and low kurtosis (Fig. 8d) are more pronounced during transition periods with moderate vertical exchange, whereas the night time cases such as Fig. 8e with the highest stability parameter ζ and least vertical exchange are less skewed and more homogeneous with respect to different sample locations. The absence of vertical exchange results in horizontally relatively homogeneous sub-canopy scalar concentrations even though there are large vertical gradients.

Figures 9 and 10 demonstrate that observed concentration offsets Δc_i can be separated into offsets which are mainly determined by instrument bias alone and into offsets which are determined by instrument bias as well as significant natural concentration differences. Figure 9a shows offset time series over two days with a succession of mixed daytime conditions (approx. 8 h to 16 h) with little scatter in the offset time series when

4402

same time accounting for vertical advection – the same arguments apply here as to avoid overestimation and noise – should give more realistic NEE estimates than those obtained from turbulent and storage flux alone.

When applying the bias correction, a balance should be found between limiting the effect of instrument drift on the gradient measurements and signal loss by potential underestimation of natural gradients. This balance can be tuned by the choice of the value for the critical mixing index MI_c . A high value of MI_c better preserves natural gradients because bias correction values are only determined from data during well mixed conditions and therefore can not eliminate natural gradients during other conditions, particularly at night when natural gradients are typically large. A low value of MI_c removes instrument drift more thoroughly since bias correction values can be found more often, i.e. from well mixed as well as partly mixed conditions. Therefore, we recommend to choose a higher MI_c the more stable the analyzer is and just low enough to allow the instrument to “survive” periods during which no bias correction values can be found (i.e. nighttime) using previously established correction values (inherited from daytime) without facing prohibitive instrument drift during those periods.

The third issue is finding the appropriate window length T_F when applying the bias correction. This is the length of the time series used to compute density distributions of concentration differences (pdf) to find their mode as outlined in Sect. 2.7. For this study the window length was chosen to be $T_F = 60$ min. The higher the instrument drift is, the shorter this window has to be in order to find a mode which is representative for the instrument bias during that time window and not affected by a significant trend of the bias. On the other hand, choosing the window as long as possible helps to preserve natural gradients which are persistent for longer periods, since persistent natural gradients with periods longer than the window length and present during non mixed conditions, and therefore affecting the mode of the pdf, are removed by the bias correction for $MI > MI_c$. However, we can conclude from the data that it is not satisfactory to choose an infinite window length (such as the time constant bias correction applied by Aubinet et al., 2003) in order to preserve natural gradients because observed instrument bias

4405

is subject to drift over time. Given the window length of 60-minutes used in the current study, the concentration difference error due to signal loss of natural concentration differences during the day has been shown to be smaller than the error of the concentration offset which would be caused by the drift of the instrument bias if the latter was corrected by a time constant bias value. Future studies should test window lengths larger than 60-minutes, particularly when using more stable analyzers.

Future work on the improvement of the bias correction approach should include a refined condition to test which data should be used when determining the pdf and the bias. Rather than using fixed 60-minute intervals to determine MI and accepting all data in a 60-minute interval satisfying $MI \geq MI_c$, a more fine grained selection of data entering the pdf can be used to select only those parts of the time series which have common properties at more than one sample point for a time period on the order of the duration of coherent structures, i.e. seconds to minutes. Among the tools which can be used to find common properties within the time series are cross correlation analysis and pattern recognition. Thereby only data with similar concentration at several sample points will enter the pdf. This helps to exclude the influence of natural gradients on the mode of the pdf, which will then be determined by instrument bias alone. Such short term correlation of time series at several sample points by tracking individual structures in the time series should be done for sample point pairs rather than using properties of the complete sample point field. These pair wise correlations then need to be linked together by choosing different configurations of sample point pairs and combining their information.

Future work can also test the applicability of the bias correction approach to sensor networks with a possibly large number of sampling points. The approach can be used when working with sensors which have a relatively high resolution but suffer from low accuracy. Whereas those sensors will deliver the fine structure (high frequency part) of the time series, the bias correction approach corrects constant and drifting instrument bias (low frequency part) and thus ensures the accuracy of the measurements.

4406

5 Conclusions

This paper has presented a measurement design capable of addressing the issue of inadequate sampling of natural concentration gradients in the temporal domain – a common characteristic of many advection measurement setups – by increasing the temporal resolution of the gradient measurements. Observing gradients with a sufficiently high temporal resolution and therefore capturing as much information as possible over a large range of temporal scales is crucial for reliable advection estimates computed from concentration gradients. In order to produce accurate gradient measurements in a multi-analyzer setup, an approach was presented which adequately addresses the problem of inter-instrument bias. It was shown that the uncertainties associated with this approach are one order of magnitude smaller compared to the benefit achieved. The proposed bias correction approach is therefore a suitable tool at least for multi-analyzer setups measuring horizontal gradients at one height, given a certain proximity of individual sampling locations. There might also be benefits from applying the bias correction approach to sequentially measured data from switching valve systems in a single-analyzer setup. It should be tested in the future whether the bias correction approach can be transferred to measurements of vertical gradients, although care has to be taken due to strong systematic vertical gradients particularly at night in the case of CO₂ concentration. The concept outlined in the current paper is not limited to measurements of CO₂ concentration but useful for the accurate observation of gradients of other scalars, too. Furthermore, it is not limited to gradient measurements for the computation of advective flux components but is worth considering for any gradient based flux measurement application. Finally, the bias correction approach is useful for the relative adjustment of signal levels between individual sensors in any kind of sensor network that samples phenomena which – at least part of the time – lead to common characteristics of the observed signal at several locations in the network.

4407

Acknowledgements. The authors wish to acknowledge the help and technical support performed by the staff of the Bayreuth Center for Ecology and Environmental Research (BayCEER) of the University of Bayreuth. The experiment was funded by the German Science Foundation (FO 226/16-1, ME2100/4-1, ZE 792/4-1). We would further like to acknowledge S. Raasch and his group for developing and providing the LES tool PALM. The LES runs were carried out on the HLRN-II-system of the HLRN (North German Alliance for Supercomputing).

References

- Aubinet, M., Heinesch, B., and Yernaux, M.: Horizontal and vertical CO₂ advection in a sloping forest, *Bound.-Lay. Meteorol.*, 108, 397–417, 2003. 4385, 4387, 4394, 4405
- Aubinet, M., Feigenwinter, C., Heinesch, B., Bernhofer, C., Canepa, E., Lindroth, A., Montagnani, L., Rebmann, C., Sedlak, P., and Gorsel, E. V.: Direct advection measurements do not help to solve the night-time CO₂ closure problem: evidence from three different forests, *Agric. For. Meteorol.*, 150, 655–664, 2010. 4385
- Baldocchi, D., Finnigan, J. J., Wilson, K., Paw U. K. T., and Falge, E.: On measuring net ecosystem carbon exchange over tall vegetation on complex terrain, *Bound.-Lay. Meteorol.*, 96, 257–291, 2000. 4385
- Baldocchi, D. D., Falge, E., Gu, L., Olson, R., Hollinger, D., Running, S., Anthoni, P., Bernhofer, C., Davis, K., Evans, R., Fuentes, J., Goldstein, A., Katul, G., Law, B., Lee, X., Malhi, Y., Meyers, T., Munger, W., Oechel, W., Paw, K. T., Pilegaard, K., Schmid, H. P., Valentini, R., Verma, S., Vesala, T., Wilson, K., and Wofsy, S.: FLUXNET: a New Tool to Study the Temporal and Spatial Variability of Ecosystem-Scale Carbon Dioxide, Water Vapor, and Energy Flux Densities, *B. Am. Meteorol. Soc.*, 82, 2415–2434, 2001. 4385
- Burns, S. P., Delany, A. C., Sun, J., Stephens, B. B., Oncley, S. P., Maclean, G. D., Semmer, S. R., Schröter, J., and Ruppert, J.: A Programmable Portable Trace-Gas Measuring System and an Evaluation of Calibration Techniques for In-Situ Carbon Dioxide Measurements, *J. Atmos. Ocean. Tech.*, 26, 291–316, 2009. 4386
- Canepa, E., Georgieva, E., Manca, G., and Feigenwinter, C.: Application of a mass consistent flow model to study the CO₂ mass balance of forests, *Agric. For. Meteorol.*, 150, 712–723, 2010. 4386
- Feigenwinter, C., Bernhofer, C., Eichelmann, U., Heinesch, B., Hertel, M., Janous, D., Kolle, O.,

4408

- Lagergren, F., Lindroth, A., Minerbi, S., Moderow, U., Molder, M., Montagnani, L., Queck, R., Rebmann, C., Vestin, P., Yernaux, M., Zeri, M., Ziegler, W., and Aubinet, M.: Comparison of horizontal and vertical advective CO₂ fluxes at three forest sites, *Agric. For. Meteorol.*, 148, 12–24, 2008. 4385
- 5 Finnigan, J.: An introduction to flux measurements in difficult conditions, *Ecol. Appl.*, 18, 1340–1350, 2008. 4385
- Foken, T., Meixner, F. X., Falge, E., Zetzsch, C., Serafimovich, A., Bargsten, A., Behrendt, T., Biermann, T., Breuning, C., Gerken, T., Hunner, M., Lehmann-Pape, L., Hens, K., Jocher, G., Kesselmeier, J., Lüers, J., Mayer, J.-C., Moravek, A., Plake, D., Riederer, M., Rütz, F., Schier, S., Siebicke, L., Sörgel, M., Staudt, K., Trebs, I., Tsokankunku, A., Wolff, V., and Zhu, Z.: Atmospheric Transport and Chemistry in Forest Ecosystems – Overview of the EGER-Project, *Agric. For. Meteorol.*, submitted, 2011. 4391
- 10 Gerstberger, P., Foken, T., and Kalbitz, K.: The Lehstenbach and Steinkreuz Catchments in NE Bavaria, Germany, in: *Biogeochemistry of Forested Catchments in a Changing Environment: A German Case Study*, edited by: Matzner, E., 172, Springer, Heidelberg, 15–41, 2004. 4388
- 15 Heinesch, B., Yernaux, M., and Aubinet, M.: Some methodological questions concerning advection measurements: a case study, *Bound.-Lay. Meteorol.*, 122, 457–478, 2007. 4394
- Kowalski, A. and Serrano-Ortiz, P.: On the relationship between the eddy covariance, the turbulent flux, and surface exchange for a trace gas such as CO₂, *Bound.-Lay. Meteorol.*, 124, 129–141, 2007. 4388
- 20 Lee, X.: On micrometeorological observations of surface-air surface exchange over tall vegetation, *Agric. For. Meteorol.*, 91, 39–49, 1998. 4385
- Mahrt, L.: Computing turbulent fluxes near the surface: Needed improvements, *Agric. For. Meteorol.*, 150, 501–509, 2010. 4386
- 25 Montagnani, L., Manca, G., Canepa, E., and Georgieva, E.: Assessing the method-specific differences in quantification of CO₂ advection at three forest sites during the ADVEX campaign, *Agric. For. Meteorol.*, 150, 702–711, 2010. 4386
- R Development Core Team: R: A Language and Environment for Statistical Computing, R Foundation for Statistical Computing, Vienna, Austria, <http://www.R-project.org>, ISBN 3-900051-07-0, 2009. 4397
- 30 Raasch, S.: PALM group available online under, <http://www.muk.uni-hannover.de/~raasch/PALM.group/PALM.group.html>, 2010. 4394
- Raasch, S. and Schröter, M.: PALM – A large-eddy simulation model performing on massively

4409

- parallel computers, *Meteorologische Zeitschrift*, 10, 363–372, 2001. 4394
- Ripley, B.: KernSmooth: functions for kernel smoothing for Wand & Jones (1995), <http://CRAN.R-project.org/package=KernSmooth>, S original by Matt Wand. R port by Brian Ripley. R package version 2.23–3, 2009. 4397
- 5 Sheather, S. J. and Jones, M. C.: A reliable data-based bandwidth selection method for kernel density estimation, *J. R. Stat. Soc., Series B*, 53, 683–690, 1991. 4397
- Siebicke, L., Serafimovich, A., and Foken, T.: Linking CO₂-advection estimates to vegetation structure at a forest site, *Agric. For. Meteorol.*, revised, 2011. 4386
- 10 Staebler, R. and Fitzjarrald, D.: Observing subcanopy CO₂ advection, *Agric. For. Meteorol.*, 122, 139–156, 2004. 4385
- Staudt, K. and Foken, T.: Documentation of reference data for the experimental areas of the Bayreuth Centre for Ecology and Environmental Research (BayCEER) at the Waldstein site, *Arbeitsergebnisse 35*, University of Bayreuth, Department of Micrometeorology, ISSN 1614–8916, 37 pp., 2007. 4388
- 15 Sun, J., Burns, S. P., Delany, A. C., Oncley, S. P., Turnipseed, A. A., Stephens, B. B., Lenschow, D. H., LeMone, M. A., Monson, R. K., and Anderson, D. E.: CO₂ transport over complex terrain, *Agric. For. Meteorol.*, 145, 1–21, 2007. 4387
- Vickers, D. and Mahrt, L.: Contrasting mean vertical motion from tilt correction methods and mass continuity, *Agric. For. Meteorol.*, 138, 93–103, 2006. 4386
- 20 Wand, M. P. and Jones, M. C.: *Kernel Smoothing*, Chapman and Hall, London, 1995. 4397

4410

Table 1. Offset statistics and error analysis for ten sample points, i.e. ten analyzers, demonstrating the correction potential of the bias correction approach (“drift span”), typical values for the maximum error possibly attributed to the bias correction approach for a “worst case” scenario (from quartile $Q_1(\Delta\text{off}_i)$ to quartile $Q_4(\Delta\text{off}_i)$) and their ratio, i.e. the relative error $\text{error}_{\text{rel}}$ according to Eq. (6). See Sect. 2.7 for definition of the terms.

Sample point	drift span [$\mu\text{mol mol}^{-1}$]	$Q_1(\Delta\text{off}_i)$ [$\mu\text{mol mol}^{-1}$]	$Q_4(\Delta\text{off}_i)$ [$\mu\text{mol mol}^{-1}$]	$\text{error}_{\text{rel}}$ []
M5	9.4	-0.46	0.41	0.09
M6	10.4	-0.86	0.72	0.15
M7	8.1	-0.53	0.47	0.12
M8	7.2	-0.7	0.49	0.16
M9	6.1	-0.36	0.41	0.13
M10	23.1	-1.11	0.93	0.09
M11	9.2	-0.89	0.66	0.17
M12	23	-0.43	0.45	0.04
M13	14.3	-0.55	0.54	0.08
M14	12.4	-0.58	0.56	0.09

4411

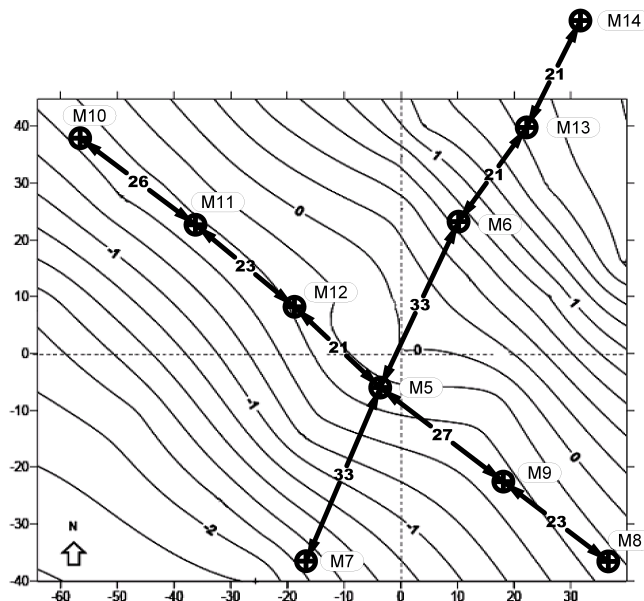


Fig. 1. Sampling locations for sub-canopy CO_2 concentration at a 2.25 m height. Distances between sampling points are given in meters. M-numbers are used for reference in the text. Topography is shown by isolines with an equidistance of 0.2 m relative to 750 m a.s.l.

4412

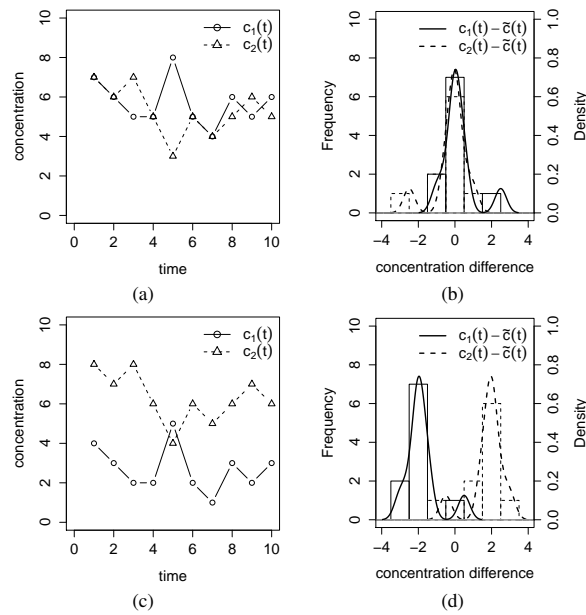


Fig. 2. Hypothetical concentration time series $c_1(t)$ and $c_2(t)$ with time $t \in [1, 10]$ (**a**, **c**), and corresponding frequency and density distributions of concentration differences $c_i(t) - \bar{c}(t)$ (**b**, **d**) for mixed conditions (**a**, **b**) and for non mixed conditions (**c**, **d**). Regarding the density distributions (**b** and **d**), the histogram bars indicate the frequency for binwidths of 1.0, the solid line is a kernel density estimation generated with the same tools which were used for density estimation of measured concentration data as described in Sect. 2.7.

4413

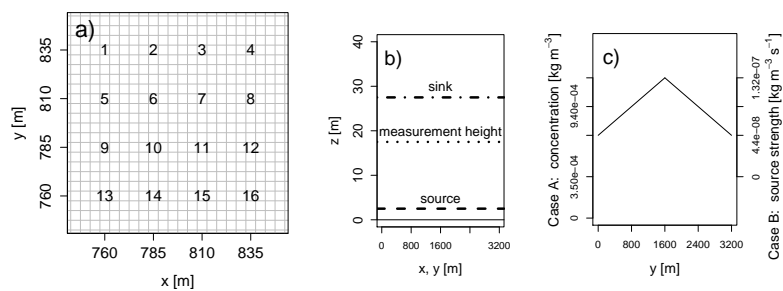


Fig. 3. Setup of Large Eddy Simulation study. Virtual sensor locations (**a**), Source-sink distribution (**b**) and background concentration gradient (**c**). Grid spacing: 5 m.

4414

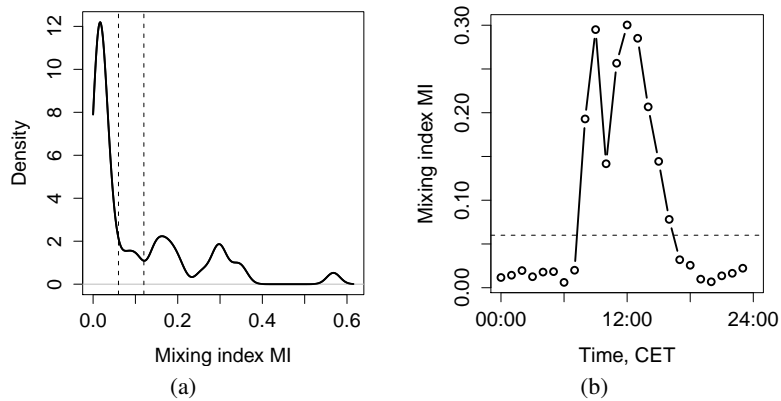


Fig. 4. (a) Density distribution of mixing index MI (solid line). Dashed lines at $MI=0.06$ and $MI=0.12$ enclose range for sensible choices of a critical mixing index MI_c . (b) Diurnal course of mixing index on 29 June 2008 (solid line) and MI_c (dashed line). MI is representative for the whole sample point field (see Sect. 2.6 for details of the calculation).

4415

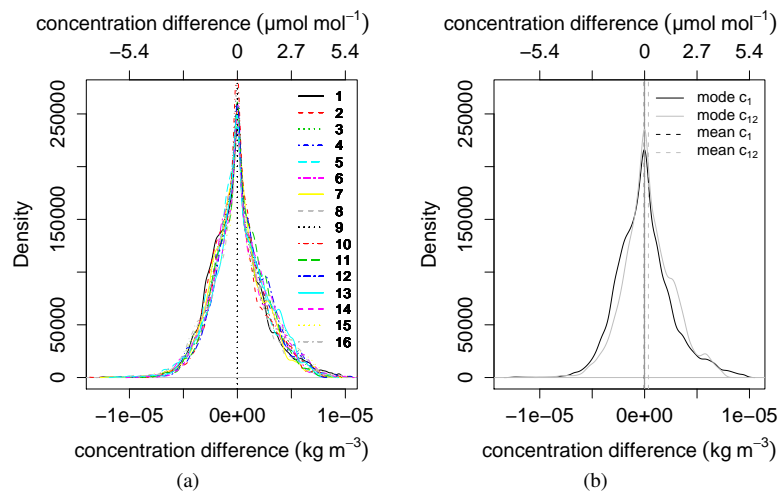


Fig. 5. Density distribution of LES modelled concentration differences $c_i(t) - \bar{c}(t)$ of a point measurement $c_i(t)$ relative to the field average concentration $\bar{c}(t)$ for concentration time series $c_1(t), c_2(t), \dots, c_{16}(t)$ and $n = 16$ sensor locations 1, 2, ..., 16 (a), and for $c_1(t)$ and $c_{12}(t)$ at sensor locations 1 and 12 (b). Note that the density distributions of $c_1(t) - \bar{c}(t)$ and $c_{12}(t) - \bar{c}(t)$ have a common mode but different mean.

4416

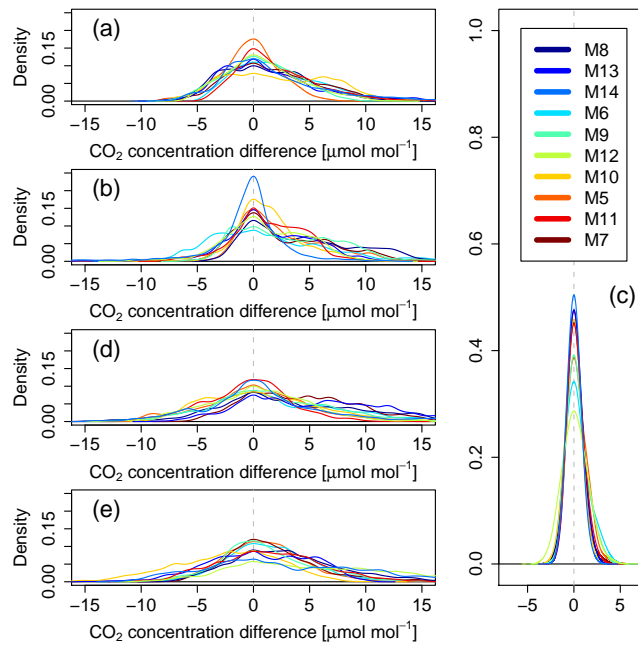


Fig. 8. Density distribution of concentration differences $c_i(t) - \bar{c}(t)$ using bias corrected measured 60-minute concentration timeseries $c_i(t)$, number of sample locations $n = 10$, for five typical cases over the course of the day on 29 June 2008 with varying stability parameter ζ (measured at a 36 m height) and mixing index MI (according to Eq. 3), night time, 01:00–02:00, $\zeta = -0.16$, $MI=0.015$ (a), night-day transition, 07:00–08:00, $\zeta = 0.65$, $MI=0.020$ (b), daytime, 12:00–13:00, $\zeta = -0.27$, $MI=0.218$ (c), day-night transition, 19:00–20:00, $\zeta = 0.06$, $MI=0.010$ (d) and nighttime with katabatic drainage flow, 22:00–23:00, $\zeta = 19.50$, $MI=0.016$ (e). Legend indicates measurement locations according to Fig. 1.

4419

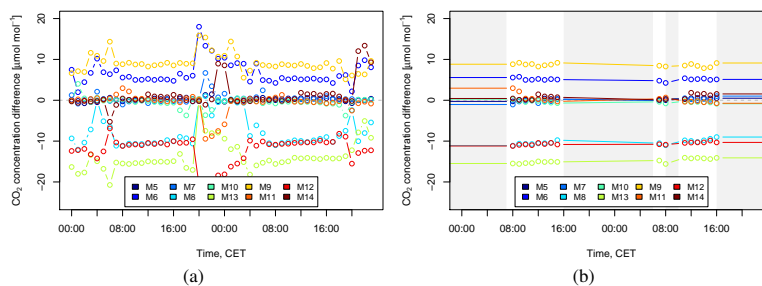


Fig. 9. Time series of the modes of density distributions of concentration differences $c_i(t) - \bar{c}(t)$ (see Fig. 7a for example distributions for one 60-minute time step) for 10 sampling locations on 29 June and 30 June 2008, (a) before filtering with mixing index, and (b) after filtering with mixing index $MI_c=0.13$. Modes from periods which satisfy $MI < MI_c$ are not used during bias correction (grey mask). The last mode at a time with $MI \geq MI_c$ is used instead (solid lines).

4420

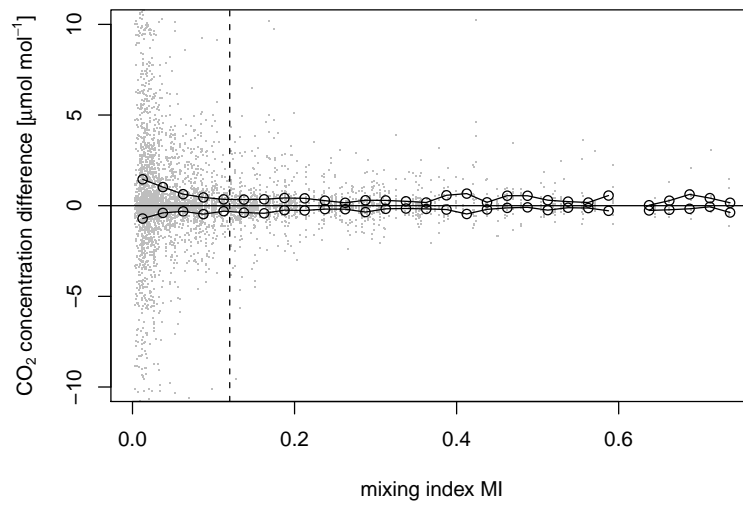


Fig. 10. Modes of 60-minute density distributions of concentration differences $c_i(t) - \bar{c}$ minus analyzer drift (mode of 24 h pdf of 60-minute modes subtracted daily) versus mixing index MI . Grey points indicate measurements, the solid line marks the 25% and 75% quantiles for mixing index binwidths of 0.025 with the circles centered at each bin. Dashed line at $MI=0.12$ indicates a sensible choice for the critical mixing index MI_c .